MATERIALS SCIENCE

Biodegradable electrospinning superhydrophilic nanofiber membranes for ultrafast oil-water separation

Xiquan Cheng[1,2]*, Tongyu Li[1], Linlin Yan[3], Yang Jiao[1], Yingjie Zhang[1,2], Kai Wang[1], Zhongjun Cheng[3], Jun Ma[4]*, Lu Shao[3]*

Although membrane technology has attracted considerable attention for oily wastewater treatment, the plastic waste generated from discarded membranes presents an immediate challenge for achieving eco-friendly separation. We designed on-demand biodegradable superhydrophilic membranes composed of polylactic acid nanofibers in conjunction with polyethylene oxide hydrogels using electrospinning technology for ultrafast purification of oily water. Our results showed that the use of the polyethylene oxide hydrogels increased the number of hydrogen bonds formed between the membrane surface and water molecules by 357.6%. This converted hydrophobic membranes into superhydrophilic ones, which prevented membrane fouling and accelerated emulsion penetration through the membranes. The oil-in-water emulsion permeance of our newly designed nanofiber membranes increased by 61.9 times (2.1×10^4 liters per square meter per hour per bar) with separation efficiency >99.6%, which was superior to state-of-the-art membranes. Moreover, the formation of hydrogen bonds was found to accelerate polylactic acid biodegradation into lactic acid by over 30%, offering a promising approach for waste membrane treatment.

INTRODUCTION

Oily wastewater is generated by domestic activities, industrial processes, and marine oil spills, and its increasing discharge has caused severe environmental pollution and endangered global ecosystems. Therefore, it is urgently necessary to develop energy-efficient and eco-friendly methods to treat oily wastewater (*1*, *2*). Conventional separation methods include gravity separation, coagulation/flocculation, skimming, and flotation (*3*–*7*). However, they have not been widely adopted for oily wastewater remediation because of their high cost and low separation efficiency toward small droplets in oil-in-water emulsions. Separation technology based on superhydrophilic membranes is an effective method to remove oil droplets from water. Superhydrophilic membranes are composed of multiscale micro/nanostructures and multihydrated functional groups, demonstrating a high separation efficiency, particularly in the treatment of wastewater containing 0.2- to 2-μm oil droplets (*8*–*11*). Previously, we developed asymmetric cross-linked polyethylene glycol (PEG)–modified polyacrylonitrile (PAN) nanofiber membranes using electrospinning technology, which showed high permeances above 2.2×10^4 liters m^{-2} $hour^{-1}$ bar^{-1}, high flux recovery rates above 98%, and low irreversible fouling rates of ~2% (*12*). Conventional polymeric membranes, such as poly(vinylidene fluoride), PAN, and polyethersulfone, have proven effective in the purification of oily wastewater as well. However, these petrochemical-based membranes are derived from fossil resources (*11*–*13*), and the membrane waste is always buried or burned, causing secondary contamination, including microplastics (*13*) and air pollutants (*14*, *15*). From this perspective, the entire remediation process is material-consuming and not sustainable (Fig. 1A). It remains challenging to find environmentally friendly approaches to purifying oily wastewater on a large scale.

To address the aforementioned issue, we focused on the biodegradable polymer polylactic acid (PLA). Lactic acid, the monomer of PLA, is a biological material and can be extracted from plants, animals, and the fermentation broth of microorganisms (*16*, *17*). PLA membranes do not produce harmful waste because PLA is degradable by specific microorganisms (Fig. 1B) and can eventually be transformed into lactic acid through biodegradation (*18*). In addition, PLA membranes are less expensive than poly(vinylidene fluoride), polyethersulfone, and other conventional membranes (*19*). Therefore, PLA is an ideal candidate to replace conventional nonrenewable petrochemical-based materials (*20*–*26*). However, PLA has poor hydrophilicity owing to its hydrophobic functional groups, such as methyl and ester groups. Oil droplets can penetrate through the membrane and easily adhere to the membrane surface and pore walls, thereby reducing its separation performance (*12*, *25*, *27*). Therefore, the surface of PLA membranes has been modified by incorporating TiO_2 nanoparticles, attempting to enhance the penetration of oily wastewater and alleviate membrane fouling (*25*, *26*). The TiO_2-incorporated PLA membranes demonstrated high oil-in-water permeance (9.5×10^3 liters m^{-2} $hour^{-1}$ bar^{-1}) and high separation efficiency (above 99%) (*25*). However, their large-scale manufacturing is challenging because of their multistep fabrication procedure, and their practical application is restricted by insufficient interactions between the TiO_2 coating and membrane.

Here, we proposed a facile strategy to fabricate a new kind of superhydrophilic on-demand degradable PLA nanofiber membranes for the ultrafast separation of oil-in-water emulsions in conjunction with biocompatible polyethylene oxide (PEO) hydrogels (*28*). The hydrogels were fabricated by adding reactive PEO

[1]State Key Laboratory of Urban Water Resource and Environment, School of Marine Science and Technology, Harbin Institute of Technology, Weihai 264209, P.R. China. [2]Shandong Sino-European Membrane Technology Research Institute Co. Ltd., Weihai Key Laboratory of Water Treatment and Membrane Technology, Weihai 264209, P.R. China. [3]MIIT Key Laboratory of Critical Materials Technology for New Energy Conversion and Storage, School of Chemical Engineering and Technology, State Key Laboratory of Urban Water Resource and Environment (SKLUWRE), Harbin Institute of Technology, Harbin 150001, P.R. China. [4]State Key Laboratory of Urban Water Resource and Environment, School of Environment, Harbin Institute of Technology, Harbin 150090, China.
*Corresponding author. Email: chengxiquan@hit.edu.cn (X.C.); majun@hit.edu.cn (J.M.); shaolu@hit.edu.cn (L.S.)

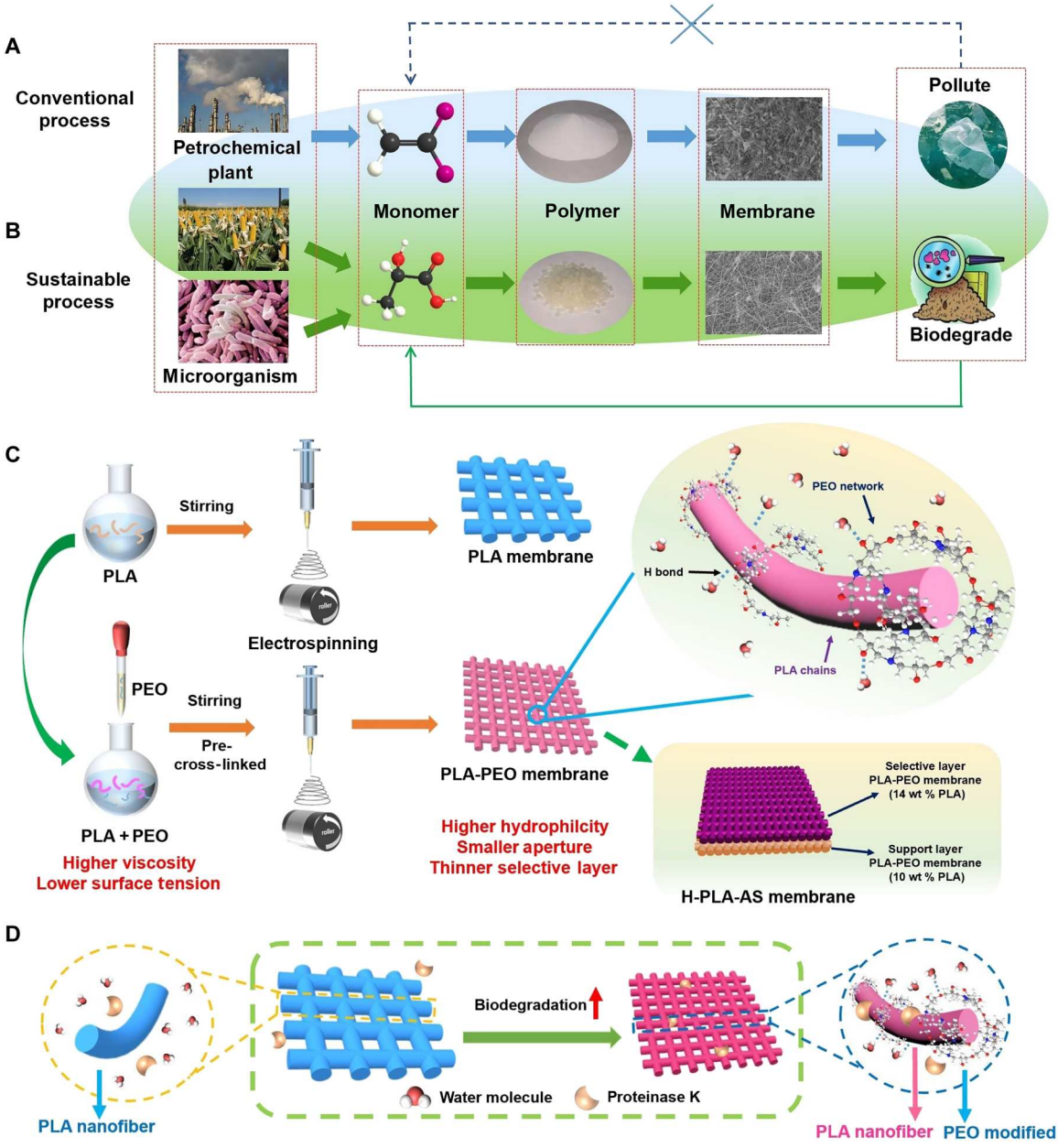

Fig. 1. Cyclic, preparation, and biodegradation processes of membranes. Cyclic process of (**A**) conventional and (**B**) sustainable membranes in nature. (**C**) Preparation of PLA-based membranes. (**D**) The biodegradation process of PLA-based nanofiber membranes.

monomers to an electrospun doping solution. During electrospinning, reactive PEO monomers modified the surface tension of the solution, thereby tailoring the morphology and structure of the cross-linked PEO-modified PLA nanofiber membranes (hereafter denoted as H-PLA). Moreover, asymmetrically cross-linked PEO-modified PLA membranes (denoted as H-PLA-AS membranes) with a thin selective layer (small pores) and support layer were designed to further reduce the mass transfer of oil-in-water emulsions. The PEO monomers could react with each other to form a PEO hydrogel with a cross-linked structure, improving the affinity between the nanofibers and water molecules and promoting the formation of hydrogen bonds (H bonds) between the surface molecules of the nanofiber membranes and water molecules. The formation of H bonds could effectively induce the transition from a hydrophobic to a superhydrophilic membrane, which promotes water penetration through the membranes while repelling oil droplets. Together with tailoring the membrane aperture (*29*), highly efficient oil-water separation membranes could be developed (Fig. 1C). Moreover, the H bonds could also increase the contact between PLA and proteinase K, accelerating the degradation of PLA (Fig. 1D). The as-prepared H-PLA-AS membrane showed excellent emulsion permeance (2.1×10^4 liters m^{-2} $hour^{-1}$ bar^{-1}), which was approximately 61.9 times higher than that of the pristine PLA membrane. Notably, the high-performance H-PLA-AS membranes showed

stable separation for oil-in-water emulsions under conventional separation conditions and could completely degrade within 1 month when exposed to proteinase K after service. Notably, the process of membrane preparation does not require additional steps. With excellent separation performance, stable performance under practical conditions and good biodegradability after treatment with specific enzymes, the H-PLA-AS nanofiber membranes show great potential to replace conventional nondegradable polymer membranes and contribute to resource conservation and environmental protection.

RESULTS

The cross-linked PEO network (hydrogels) was synthesized in situ via the ring-opening reaction of end-capping amino and epoxy groups in active additives (*30*). Notably, the concentration and composition of the doping solutions had a great impact on the structure and separation performance of the nanofiber membranes, as discussed in detail in the Supplementary Materials (figs. S1 to S4 and tables S1 to S3). In the cross-linked PEO hydrogel–modified PLA membranes, the PLA chains could be tightly entangled by PEO hydrogels, and the intermolecular forces between different PLA chains were modulated (*31*). Compared with the pristine PLA nanofiber membrane, H-PLA membranes showed a lower glass transition temperature (T_g), cold crystallization temperature (T_c), and melting temperature (T_m), as determined through differential scanning calorimetry (DSC) curves (Fig. 2A and table S4). The DSC results indicated that the PLA nanofiber membrane was composed of a partially crystalline structure. Moreover, the degree of crystallinity (χ_c) of H-PLA membranes increased from 2% (pristine PLA) to 15.4% (table S4). This change was possible because the PEO hydrogels with a lower molecular weight improved the diffusion ability, which could facilitate the folding and arrangement of PLA molecular chains into regular structures (*32*) and enhance the interactions between the PLA chains and PEO hydrogels. Meanwhile, the x-ray diffraction patterns of the PLA and H-PLA nanofiber membranes (fig. S5) exhibited characteristic diffraction peaks at 14.8°, 16.6°, 18.9°, and 22.2°, corresponding to the (010), (200)/(110), (203), and (105) planes of PLA, respectively (*33*, *34*). These results suggest that PLA nanofiber membranes typically consist of orthorhombic crystals owing to the orientation of PLA chains at the molecular scale during the electrospinning process (*35*). Comparatively, the full width at half maximum of the H-PLA peaks increased when the PEO hydrogels were introduced owing to the formation of irregular or defective crystals. To further verify these results, we used Fourier transform infrared (FTIR) spectroscopy to analyze the composition of PLA-based membranes (fig. S6). In comparison with that of the pristine PLA membranes, the intensity of the FTIR peak at 1181 cm^{-1} (—C—O— stretching vibrations) decreased for H-PLA. In addition, the peak at 1266 cm^{-1} disappeared, and a new peak emerged at 1211 cm^{-1} owing to the incorporation of PEO hydrogels. In the x-ray photoelectron spectroscopy spectra, the presence of C—N (285.5 eV) and N (399.6 eV) peaks indicated that PEO hydrogels were successfully introduced into the H-PLA membrane (fig. S7). When mixing PEO additives with the PLA solution, PEO molecules can be inserted into the PLA chains, reducing the van der Waals forces between the PLA chain segments. As a result, PLA-PEO solutions exhibited a higher viscosity (increased by 63.1%) and lower surface tension (decreased by 91.8%) than the pristine PLA solution (Fig. 2B) (*36*).

The pore size of the pristine PLA nanofiber membrane was approximately 2.5 μm, which decreased to 1.9 μm after incorporating

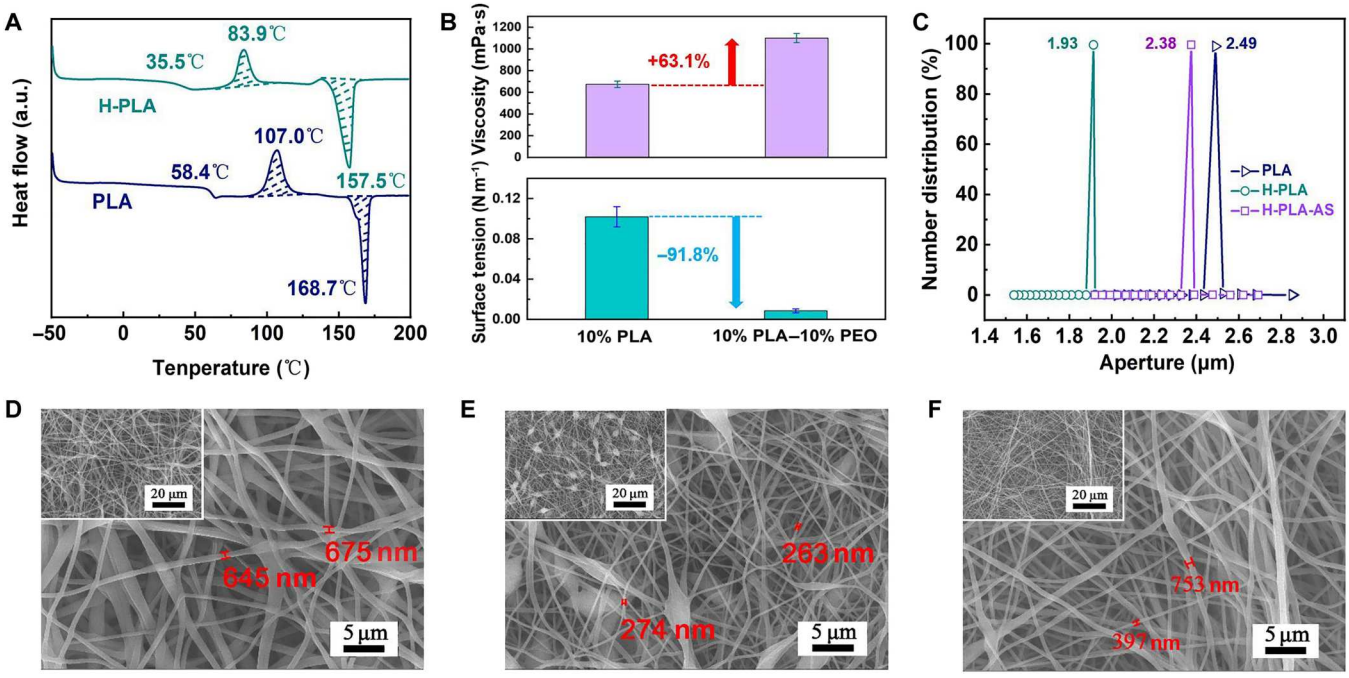

Fig. 2. The membrane structure and viscosity of the doping solutions. (**A**) DSC curves. a.u., arbitrary units. (**B**) Viscosity and surface tension of 10 wt % of PLA solution and 10 wt % of PLA–10 wt % of PEO solution. (**C**) Pore size distribution of the PLA-based membranes. Field-emission scanning electron microscopy micrographs showing the surfaces of (**D**) the PLA membrane (10 wt % of PLA), (**E**) the selective layer, and (**F**) supporting layer of the H-PLA-AS membrane (14 wt % of PLA–10 wt % of PEO).

PEO hydrogels (Fig. 2C). It was noteworthy that the average effective pore size of the H-PLA-AS membrane was larger than that of the H-PLA membrane owing to the thinner selective layer. Notably, the porosity of these PLA-based nanofiber membranes was approximately 80% (fig. S8). The cross-sectional field-emission scanning electron microscopy images of the PLA and H-PLA membranes with a thickness of approximately 80.2 μm showed uniform nanofiber stacking structures (fig. S9). The H-PLA-AS membranes were also prepared using a similar electrospinning method to tailor the membrane aperture. The thickness of the H-PLA-AS membrane was approximately 81.4 μm, including a selective layer (14.3 μm) and a support layer (67.1 μm) (fig. S9C). For PLA membranes, smooth nanofibers with a diameter of 660 ± 44 nm were stacked into a porous structure (Fig. 2D). In contrast, micrometer bead–like structures were observed in the H-PLA membranes (Fig. 2E). The same selective layer structure of the H-PLA-AS and H-PLA membranes also resulted in a similar surface morphology (Fig. 2, E and F). Notably, incorporation of PEO hydrogels resulted in a slight increase in the membrane roughness from 1.2 to 1.4 μm (fig. S10), pertaining to both bead structures and asymmetric stacking (*37*). Moreover, N signals were evenly distributed on the surface of the H-PLA-AS membrane, proving that the PEO hydrogels were intertwined with the PLA nanofibers (fig. S11 and table S5). The comparison of Fig. 2 (D and E) indicates that the diameter of the nanofibers decreased by 60% (264 ± 19 nm) after introducing the reactive PEO monomer as an additive, resulting in a smaller pore diameter (Fig. 2C) (*38*).

As mentioned above, the PEO molecules could entangle with the PLA molecules during phase inversion during the electrospinning process, introducing multiple hydrophilic functional groups, such as CH_2—O—CH_2 and —OH, on the surface of the H-PLA membranes (*12*). From the chemical element content and the FTIR spectra of the membranes (fig. S6 and table S5), the composition of the PLA-based nanofiber membranes is homogenous. To investigate the interaction between the surface molecules of PLA-based membranes and water molecules, we conducted molecular dynamics simulations (Fig. 3, A and B), as mentioned in the Supplementary Materials. As a result, the number of hydrogen bonds increased by 357.6% after the incorporation of PEO hydrogels (table S6). The 86.1% increase in the H bonds was attributed to H bonds between PLA molecules and water, while only a 13.9% increase in H bonds was attributed to H bonds between PEO hydrogels and water. As a hydrophilic polymer containing multiple ether oxygen groups and hydroxyl-terminated groups, the PEO hydrogels could interact with water molecules through H bonds, bringing water molecules closer to PLA like a "water pump" and promoting the formation of H bonds between PLA and water molecules (Fig. 3C). In addition to providing hydrophilic groups, the PEO network limited the movement of water molecules between PEO and PLA. Since the number of PLA repeat units on the membrane surface is substantially higher than that of PEO repeat units, the final increment of H bonds between the PLA and water molecules is more than that between PEO hydrogels and water. As a result, the great increase in interaction between surface molecules of PLA-based membranes and water molecules might induce the transformation from a hydrophobic toward a superhydrophilic surface. The pristine PLA nanofiber membranes exhibited high initial and stable water contact angles of approximately 119° to 131°, suggesting their strong hydrophobic features. After introducing the PEO hydrogels, the H-PLA and H-PLA-AS membranes could be completely wetted in 2.1 and 0.9 s, respectively, verifying the results of molecular dynamics simulations (Fig. 3D). The water sorption results of the PLA-based membranes (Fig. 3F) further confirm the simulation findings. The adsorption capacity of the H-PLA-AS membrane was the highest (650.1 mg cm^{-3}), which was approximately three times higher than that of the PLA membrane. This could be attributed to the increase in H bonds caused by the introduction of PEO hydrogels, as mentioned above. Moreover, DSC curves were obtained to analyze the thermodynamic behavior of the water components in the membranes. After introducing PEO hydrogels, the endothermic peak of the water-melting process shifted to a higher temperature, indicating a higher melting enthalpy (Fig. 3G). Correspondingly, the content of nonrefrigerated water in the H-PLA-AS membrane was calculated as 72.1%, indicating that the increase in H bonds provided the H-PLA-AS membrane with the strongest affinity for water, explaining its highest hydration capacity (*39*). Notably, the H-PLA-AS membranes exhibited a more superhydrophilic surface, which could be due to the highly rough asymmetric and bead-like structures (*40*). Although the hydrogels promoted the interaction between water and the PLA-based membranes, the porosity of all of the PLA-based nanofiber membranes (fig. S8) was similar and remained stable after water sorption, indicating that changes in the membrane structure caused by water sorption were not obvious. This promoted the formation of H bonds between the water molecules and PLA and improved membrane hydrophilicity (Fig. 3, B and C), which induced the transformation. Notably, the increase in the surface hydrophilicity caused by the increase in H bonds increases the driving forces of the water (join forces of the Laplace force and gravity), which might lead to a reduction in the mass-transfer resistance across the membranes.

Moreover, the pristine PLA nanofiber membrane exhibited extremely high lipophilicity and oil adsorption. The underwater oil contact angle (UWOCA) of the PLA membrane was 0°, indicating that the membrane could be rapidly wetted by oil. The UWOCAs of the H-PLA and H-PLA-AS membranes reached 151.7° and 154.7°, respectively, suggesting that oil droplets could not be adsorbed (Fig. 3D) and showing their potentially high separation efficiency in oil-in-water emulsions. As the PLA nanofiber membrane showed hydrophobic properties, the oil droplet could not slide off the surface of the membrane. However, the sliding angles of oil droplets of the H-PLA and H-PLA-AS membranes were 6.7° and 5.8°, respectively (table S7). The incorporation of PEO hydrogels also affected the surface charge, which was a critical factor that determined the performance of PLA-based membranes (fig. S12). The PLA membrane showed a negative surface charge at all tested pH values owing to the presence of highly negative carboxyl groups. After incorporating the PEO hydrogels, the point of zero charge (PZC) of the H-PLA and H-PLA-AS membranes was measured at pH 4.6 and 5.1, respectively. The shift in PZC was attributed to the change in surface groups (*41*). Accordingly, the high density of basic groups (tertiary amine group) in the PEO hydrogels might inhibit the complete dissociation of acidic groups (carboxyl group) in the membranes owing to electrostatic repulsion. Consequently, positive charges appeared on both the H-PLA and H-PLA-AS membrane surfaces, leading to positive zeta potentials at pH values lower than the PZC. In addition, the decrease in droplet charge attraction caused by the low absolute value of the zeta potential of the modified membrane may alleviate membrane fouling (figs. S12 and S13)

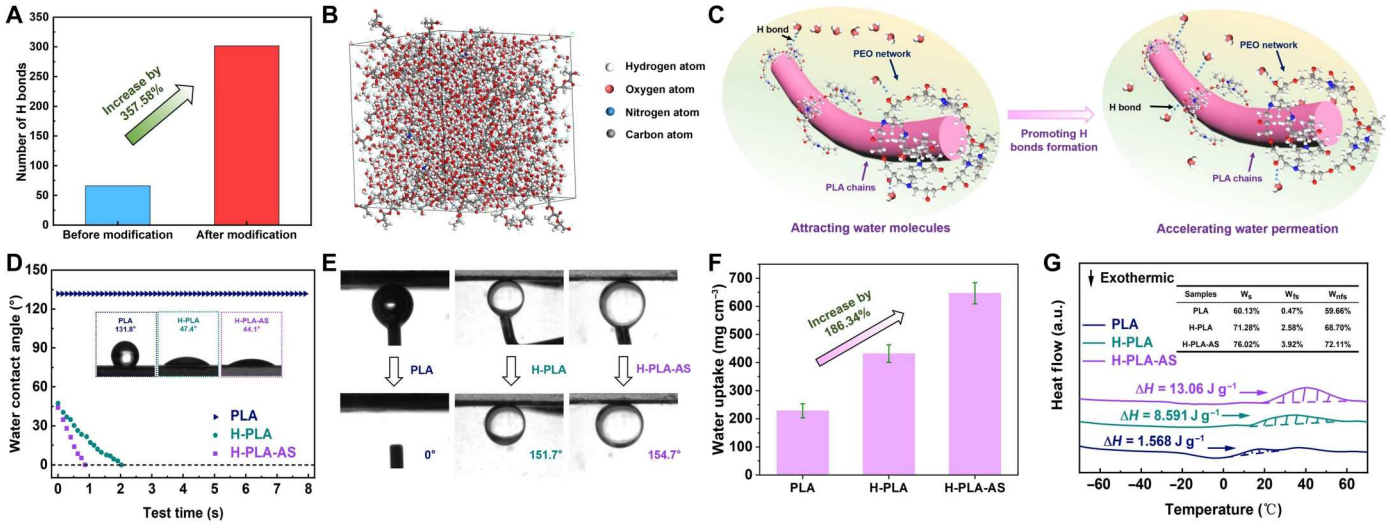

Fig. 3. Properties of PLA-based membranes. (**A**) Number of H bonds formed in the solution system before and after modification. (**B**) Three-dimensional model of the H_2O-PLA-PEO system. (**C**) The possible mechanism by which hydrogels promote the formation of H bonds between water and the membrane surface. (**D**) Dynamic water contact angle on the surface of the membranes (insets are the optical images of water droplets on PLA-based membranes). (**E**) Optical images of UWOCA on membrane surfaces. (**F**) Water uptake capability of PLA-based membranes. (**G**) DSC curves of different membranes showing the presence of water in the membranes (insets are the percentages of different forms of water in the membrane). Ws, relative water absorption ration of the mebrane; Wfs and Wnfs, content of frozen and nonfrozen bound water in the membrane, respectively.

(*42*). Overall, because of the presence of biocompatible PEO hydrogels and the increment of hydrated hydrogen bonds, the H-PLA and H-PLA-AS membranes have a porous structure, hydrophilicity, and modified surface charges, which might help achieve comprehensive separation performance toward oil-in-water emulsions.

Because of the intrinsic hydrophobic surface, the pristine PLA nanofiber membranes showed low emulsion permeance (330.4 liters m^{-2} $hour^{-1}$ bar^{-1}) and oil separation efficiency (93.9%). After filtration with PLA membranes, a large amount of oil remained in the filtrate (fig. S14). In contrast, both the permeance and separation efficiency increased greatly after incorporating the PEO hydrogels into the PLA membranes. The improvement was because the abundant H bonds between the PLA and H_2O induced the reversal of the wetting property on the H-PLA-AS membrane surface (*43*). Moreover, the enhanced compatibility with water, fine-tuned pore structures, and surface charges caused by the introduction of the PEO hydrogels contributed to the improvement of the separation performance. The emulsion permeance of the H-PLA-AS membrane increased by 61.9 times compared to that of the pristine PLA membrane, with an outstanding separation efficiency of 99.6% (Fig. 4A). Notably, before filtration, the feed emulsion was opaque with oil droplets larger than 1000 nm, while the filtrate appeared clear and transparent with oil droplets smaller than 100 nm (Fig. 4B and fig. S15). As the average pore size of the H-PLA-AS membrane was approximately 2.4 μm, the pore size exclusion effects were not the main factor in the oil-water separation process. Oil droplets larger than 150 nm could not pass through the membrane because of Laplace repulsion (*44*). Because the H-PLA and H-PLA-AS membranes could not be wetted by the oil droplets, the Laplace force (capillary force, $\frac{2\gamma}{r}\cos\theta$, where θ represents oil contact angle) could prevent droplets from passing through the membrane. In addition, compared with the pristine PLA membrane, the permeance of the symmetrical H-PLA membrane decreased, and the separation efficiency of oil droplets increased slightly, which might be related to the increase in the mass transfer resistance and the decrease in pore size. The pristine PLA nanofiber membrane showed poor cyclic stability (fig. S16). With the increase in the cycle number, the permeance increased, and the separation performance decreased, which was caused by the wetting of the hydrophobic membranes by oil droplets during the measurement. Moreover, fouling was evident on the surface of the PLA membrane (fig. S13), while H-PLA-AS showed less tendency to be fouled by oil droplets. Compared with the oil-water separation membranes reported previously (*3*, *45*–*57*), PEO in H-PLA-AS membranes increased the number of hydrogen bonds, thus enhancing the hydrophilicity and permeance to water (Table 1). Notably, because the H-PLA-AS membranes demonstrated a superhydrophilic surface with multiple H bonds, the rejection of emulsions was less dependent on the type of surfactant (figs. S17 and S18). In addition, the thinner selective layer also played an important role in the increase in permeance (Fig. 4D). Notably, the separation performance of the H-PLA-AS nanofiber membranes and PLA membranes was stable within 4 weeks (Fig. 4C), implying no degradation under the general operating conditions in water.

Although PLA is a well-known biodegradable material, its biodegradation requires specific conditions (*58*, *59*). PLA biodegradation mainly occurs through an enzymatic hydrolysis process under alkaline conditions (*58*). In the current work, the biodegradability of PLA and H-PLA-AS membranes in the presence of proteinase K was investigated. It was noteworthy that H-PLA-AS membranes completely degraded within a week with the disappearance of bead-like structures. However, pristine PLA membranes took approximately 10 days. After further analysis, the main degradation product was found to be lactic acid (figs. S19 and S20), which is an intermediate product of animal and plant metabolism (*16*, *17*). These findings indicate that the membranes could be degraded on-

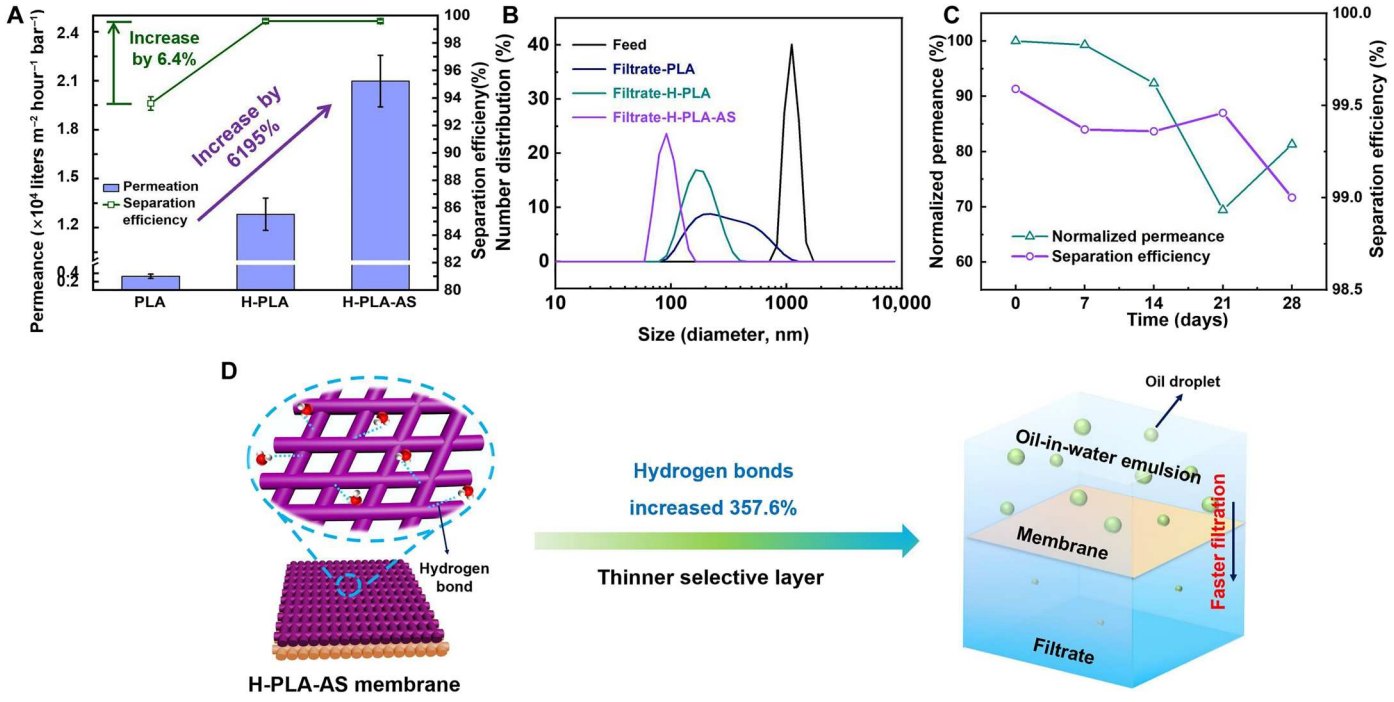

Fig. 4. Separation performance and possible separation mechanism of PLA-based membranes. (**A**) Separation performance of PLA-based membranes for *n*-octane–in–water emulsions. (**B**) Emulsion particle size distribution before and after filtration. (**C**) The stability of H-PLA-AS nanofiber membranes (the initial permeation is set as 100%). (**D**) The possible mechanism of the improvement in permeance of H-PLA-AS membranes.

demand after service. The cross-linked PEO network in the membrane increased the binding ability of protease K to the nanofibers while also providing numerous binding sites for the formation of hydrogen bonds.

Therefore, we believe that these factors accelerated the biodegradation rate of the modified membrane in an aqueous environment. Further experiments on the degradation of membranes in aqueous solutions at different pH values revealed that a strongly alkaline environment could further accelerate the degradation of the H-PLA-AS membranes into lactic acid (figs. S21 and S22).

DISCUSSION

For ultrafast and highly efficient separation of oily wastewater, we designed a new kind of biodegradable nanofiber membrane (H-PLA-AS) through an electrospinning technique. Under a high-voltage electrostatic field, an asymmetric porous structure with a large-pore support layer and a small-pore selective layer was formed by stepwise electrospinning of doping solutions consisting of different concentrations of PLA and hydrophilic reactive monomers. After that, the hydrophilic reactive monomers were cross-linked to form PEO hydrogels to achieve a superhydrophilic surface. Notably, both PLA and PEO hydrogels are biofriendly materials that show strong promise in substituting conventional petroleum-based nonbiodegradable membranes.

Compared with the state-of-the-art membranes reported previously (Table 1) (*3*, *45*–*57*), the H-PLA-AS membranes demonstrated the best comprehensive separation performance. When separating surfactant-stabilized oil-in-water emulsions, the H-PLA-AS membranes showed at least 25% higher permeance (2.1 $\times 10^4$ liters m^{-2} $hour^{-1}$ bar^{-1}) and comparable separation efficiency of approximately 99.6% and could completely remove oil droplets smaller than 150 nm. The reason why the H-PLA-AS membranes had both high permeance and separation efficiency could be attributed to their thin selective layer, appropriate average pore size (2.4 μm), and superhydrophilic surface (Fig. 4D). Among these factors, the superhydrophilic surface caused by the increased H bonds through introducing the PEO hydrogels plays a dominant role in the ultrafast mass transfer across the membranes. On the one hand, the H bonds could promote water molecules penetrating through the nanofiber membranes, which accounted for the increment in permeance. On the other hand, the PEO hydrogels provide multistage hydrophilic functional groups such as CH_2—O—CH_2 and —OH, resulting in the transformation of the hydrophobic surface toward superhydrophilic ones. Because of the superhydrophilic surface and appropriate pore size, the H-PLA-AS membranes could repel oil droplets according to the Laplace equations (*44*). Notably, the permeance and separation efficiency of the pristine PLA nanofiber membranes with similar porous structures were much lower than those of the H-PLA-A membranes, which also confirms the inferences.

As a potential alternative to commercial ultrafiltration membranes for oily wastewater separation, H-PLA-AS demonstrated stable separation performance and excellent antifouling performance and could be degraded by proteinase K on demand after service. These excellent properties benefited from the introduction of PEO hydrogels into the nanofiber membranes. As mentioned above, the cross-linked PEO network provided stable chemical stability and multiple hydrophilic functional groups, promoting the stable separation performance and antifouling performance of

Table 1. Comparison of the separation performance between our membrane and the state of the art membranes reported in the literature (*3*, *45*–*57*).

Membrane	Reference	Permeance ($\times 10^4$ liters m^{-2} $hour^{-1}$ bar^{-1})	Separation efficiency (%)	Oil	Surfactant
H-PLA-AS	This work	2.1	99.6	*n*-octane	SDS
Pristine PLA	This work	0.033	93.9	*n*-octane	SDS
Vermiculite membrane	Huang *et al.* (*3*)	0.7	95.5	Kerosene/hexane/ petroleum ether/ vegetable oil	Sodium dodecylbenzenesulfonate
$(TBP)_4SiW$@BCB gel membrane	Zhang *et al.* (*45*)	0.35	99.5	*n*-hexane	–
PAN-based membrane	Cheng *et al.* (*46*)	1.7	99.6	*n*-octane	Span 80
$Cu_3(PO_4)_2$ nanosheets-wrapped mesh membrane	Zhang *et al.* (*47*)	0.45	99.9	Crude oil	–
Wood nanotechnology–based membrane	Kim *et al.* (*48*)	0.046	99.4	Hexane	SDS
$Al_{18}B_4O_{33}$-coated alumina structure	Chen *et al.* (*49*)	0.015	99.7	Hexane/octane/ cyclohexane	SDS
Graphene oxide-based membrane	Cai *et al.* (*50*)	0.46	95.0	Hexane	SDS
2-(Dimethylamino)ethyl methacrylate–based membrane	Joo *et al.* (*51*)	2.3	99.0	Hexane/hexadecane	–
ZIF-8@rGO@Sponge	Gu *et al.* (*52*)	0.99	99.8	*n*-heptane	–
Covalent organic frameworks (COFs)-based membrane	Liu *et al.* (*53*)	2.8	99.5	*n*-heptane/cyclohexane	–
Nanofibrous cellulosic (NFC) membrane	Hong *et al.* (*54*)	2.0	99.0	Mineral oil/*n*-hexane	–
PAN-based membrane	Ge *et al.* (*55*)	0.52	99.9	*n*-hexane/diesel	SDS
Polydimethylsiloxane-Fe_3O_4@MF sponge	Liu *et al.* (*56*)	1.4	98.7	Soybean oil/diesel	Span 80
Wrinkle-petterned microparticles (WPM)-based membrane	Zhao *et al.* (*57*)	0.72	99.6	Crude oil	Tween 80

the membranes. When the H-PLA-AS membranes were treated with proteinase K after service, the PEO hydrogels promoted the binding ability of protease K to the nanofibers through increased H bonds (Fig. 1D), thereby accelerating the biodegradation process (less than one week). Notably, the main degradation product was found to be lactic acid, which could be reused by organisms. In conclusion, we provided a facile approach to developing biodegradable superhydrophilic PLA–based nanofiber membranes through the electrospinning technique. Considering that organic solvents can be recovered through a vacuum system during electrospinning, the electrospinning process may become a green and revolutionary supplement to the phase inversion technique to develop separation membranes for oily wastewater treatment.

MATERIALS AND METHODS

Preparation of PLA membranes

Briefly, dried PLA resins were dissolved in a solvent mixture of dioxane and *N*-methyl pyrrolidone at a mass ratio of 1:1 to obtain a PLA solution of 10 wt %. After preparation, a disposable syringe was filled with the PLA solution and transferred to the electrospinning equipment. The following operating parameters were used for the electrospinning of PLA membranes. The positive and negative voltages were set at 15 kV and −2000 V, respectively. A stainless steel needle type 1.2# with an inner diameter of 0.9 mm was used for the injection of the PLA solution at an injection rate of 0.0010 mm s^{-1}. The distance between the drum collector and the needle was set to 18 cm. In addition, electrospinning was carried out for 10 hours at a scanning rate of 0.4 cm s^{-1} and a drum speed of 171 rpm. After electrospinning, the membranes were heat-treated in an oven at 100°C for 2 hours to obtain pure PLA nanofiber membranes.

Preparation of H-PLA membranes

First, a certain amount of PEG diglycidyl ether (PEGDGE) was dispersed in a solvent mixture containing dioxane/*N*-methyl pyrrolidone (mass ratio, 1:1) by heating at 70°C and stirring, followed by the addition of PLA. After cooling the mixture to approximately 25°C, polyetheramine (PEA) was added under stirring. The final mass ratio of PEA to PEGDGE was 1:2, and the total amount of PLA in the mixture was 10 wt %. Subsequently, the prepared mixture was used for electrospinning using the same parameters as described for the preparation of PLA membranes. Similarly, the electrospun nanofiber membranes were then heated in an oven at 100°C for 2 hours to obtain a PLA nanofiber membrane

modified by the crosslinked PEO network (denoted as the H-PLA membrane).

Preparation of H-PLA-AS membranes

First, a PLA-based support layer was prepared. Similar to the preparation of H-PLA membranes, a PLA-PEO solution containing 14 wt % of PLA was prepared using a mixture of PEA and PEGDGE. The electrospinning parameters were similar to those used for the preparation of PLA membranes, except for the shorter spinning time of 8 hours. For the electrospinning of the selective layer, the PLA-PEO solution containing 10 wt % of PLA was used with a spinning time of 2 hours. Last, the electrospun membranes were heat-treated in an oven at 100°C for 2 hours to obtain asymmetric PLA composite nanofiber membranes (denoted as the H-PLA-AS membrane).

Supplementary Materials

This PDF file includes:

Supplementary Text
Figs. S1 to S22
Tables S1 to S7
References

REFERENCES AND NOTES

1. D. Jassby, T. Y. Cath, H. Buisson, The role of nanotechnology in industrial water treatment. *Nat. Nanotechnol.* **13**, 670–672 (2018).
2. D. Lewis, How Mauritius is cleaning up after major oil spill in biodiversity hotspot. *Nature* **585**, 172 (2020).
3. K. Huang, P. Rowe, C. Chi, V. Sreepa, T. Bohn, K.-G. Zhou, Y. Su, E. Prestat, P. Balakrishna Pillai, C. T. Cherian, A. Michaelides, R. R. Nair, Cation-controlled wetting properties of vermiculite membranes and its promise for fouling resistant oil–water separation. *Nat. Commun.* **11**, 1097 (2020).
4. J. N. Murphy, C. M. Schneider, K. Hawboldt, F. M. Kerton, Hard to soft: Biogenic absorbent sponge-like material from waste mussel shells. *Matter* **3**, 2029–2041 (2020).
5. P. Cherukupally, W. Sun, A. P. Wong, D. R. Williams, G. A. Ozin, A. M. Bilton, C. B. Park, Surface-engineered sponges for recovery of crude oil microdroplets from wastewater. *Nat. Sustain.* **3**, 136–143 (2020).
6. A. Alammar, S. H. Park, C. J. Williams, B. Derby, G. Szekely, Oil-in-water separation with graphene-based nanocomposite membranes for produced water treatment. *J. Membr. Sci.* **603**, 118007 (2020).
7. C. Wang, Y. Lü, C. Song, D. Zhang, F. Rong, L. He, Separation of emulsified crude oil from produced water by gas flotation: A review. *Sci. Total. Environ.* **845**, 157304 (2022).
8. Z. Wang, M. Elimelech, S. Lin, Environmental applications of interfacial materials with special wettability. *Environ. Sci. Technol.* **50**, 2132–2150 (2016).
9. Z. Wang, H. C. Yang, F. He, S. Peng, Y. Li, L. Shao, S. B. Darling, Mussel-inspired surface engineering for water-remediation materials. *Matter* **1**, 115–155 (2019).
10. H. Dai, Z. Dong, L. Jiang, Directional liquid dynamics of interfaces with superwettability. *Sci. Adv.* **6**, eabb5528 (2020).
11. X. Li, Q. Gui, Y. Wei, L. Feng, Novel superwetting nanofibrous skins for removing stubborn soluble oil in emulsified wastewater. *J. Mater. Chem. A.* **9**, 26127–26134 (2021).
12. X. Q. Cheng, Z. Sun, X. Yang, Z. Li, Y. Zhang, P. Wang, H. Liang, J. Ma, L. Shao, Construction of superhydrophilic hierarchical polyacrylonitrile nanofiber membranes by in situ asymmetry engineering for unprecedently ultrafast oil–water emulsion separation. *J. Mater. Chem. A.* **8**, 16933–16942 (2020).
13. Y. Li, D. Yuan, Q. Geng, X. Yang, H. Wu, Y. Xie, L. Wang, X. Ning, J. Ming, MOF-embedded bifunctional composite nanofiber membranes with a tunable hierarchical structure for high-efficiency $PM_{0.3}$ purification and oil/water separation. *ACS. Appl. Mater. Inter.* **13**, 39831–39843 (2021).
14. K. L. Law, R. Narayan, Reducing environmental plastic pollution by designing polymer materials for managed end-of-life. *Nat. Rev. Mater.* **7**, 104–116 (2022).
15. D. M. Mitrano, W. Wohlleben, Microplastic regulation should be more precise to incentivize both innovation and environmental safety. *Nat. Commun.* **11**, 5324 (2020).
16. S. K. Ramamoorthy, M. Skrifvars, A. Persson, A review of natural fibers used in biocomposites: Plant, animal and regenerated cellulose fibers. *Polym. Rev.* **55**, 107–162 (2015).
17. B. Khoshnevisan, M. Tabatabaei, P. Tsapekos, S. Rafiee, M. Aghbashlo, S. Lindeneg, I. Angelidaki, Environmental life cycle assessment of different biorefinery platforms valorizing municipal solid waste to bioenergy, microbial protein, lactic and succinic acid. *Renew. Sust. Energ. Rev.* **117**, 109493 (2020).
18. R. E. Drumright, P. R. Gruber, D. E. Henton, Polylactic acid technology. *Adv. Mater.* **12**, 1841–1846 (2000).
19. M. Dusselier, P. Van Wouwe, A. Dewaele, P. A. Jacobs, B. F. Sels, Shape-selective zeolite catalysis for bioplastics production. *Science* **349**, 78–80 (2015).
20. S. Zhou, L. Jiang, Z. Dong, Overflow control for sustainable development by superwetting surface with biomimetic structure. *Chem. Rev.* **123**, 2276–2310 (2023).
21. R. A. Sheldon, Metrics of green chemistry and sustainability: Past, present, and future. *ACS. Sustain. Chem. Eng.* **6**, 32–48 (2018).
22. A. K. Mohanty, S. Vivekanandhan, J. M. Pin, M. Misra, Composites from renewable and sustainable resources: Challenges and innovations. *Science* **362**, 536–542 (2018).
23. L. Chang, D. Wang, Z. Cao, C. Liu, J. Yang, X. Zhang, Y. Tian, H. Liu, L. Jiang, Miscible organic liquid separation of superwetting membrane driven by synergistic polar/nonpolar interactions. *Matter* **5**, 1251–1262 (2022).
24. Y. Zhang, J. Jing, T. Liu, L. Xi, T. Sai, S. Ran, Z. Fang, S. Huo, P. Song, A molecularly engineered bioderived polyphosphate for enhanced flame retardant, UV-blocking and mechanical properties of poly (lactic acid). *Chem. Eng. J.* **411**, 128493 (2021).
25. Z. M. Zhang, Z. Q. Gan, R. Y. Bao, K. Ke, Z. Y. Liu, M. B. Yang, W. Yang, Green and robust superhydrophilic electrospun stereocomplex polylactide membranes: Multi-functional oil/water separation and self-cleaning. *J. Membr. Sci.* **593**, 117420 (2020).
26. Z. Xiong, H. Lin, Y. Zhong, Y. Qin, T. Li, F. Liu, Robust superhydrophilic polylactide (PLA) membranes with a TiO_2 nano-particle inlaid surface for oil/water separation. *J. Mater. Chem. A.* **5**, 6538–6545 (2017).
27. Z. K. Sun, Y. Zhou, Y. Jiao, X. Q. Cheng, Y. Zhang, P. Wang, H. Liang, X. Yang, E. Drioli, A. Figoli, J. Ma, L. Shao, Multi-hydrophilic functional network enables porous membranes excellent anti-fouling performance for highly efficient water remediation. *J. Membr. Sci.* **608**, 118191 (2020).
28. X. Li, J. Yang, B. Xue, C. Zhang, L. Shi, C. Wu, Y. Su, X. Jin, Y. Liu, X. Zhu, Molecular insights for the biological interactions between polyethylene glycol and cells. *Biomaterials* **147**, 1–13 (2017).
29. W. Zhang, N. Liu, Q. Zhang, R. Qu, Y. Liu, X. Li, Y. Wei, L. Feng, L. Jiang, Thermo-driven controllable emulsion separation by a polymer-decorated membrane with switchable wettability. *Angew. Chem. Int. Ed.* **130**, 5842–5847 (2018).
30. S. Wang, Q. Sun, Y. Ma, Z. Wang, H. Zhang, X. Shi, D. Song, L. Zhang, L. Zhu, Dual in situ polymerization strategy endowing rapid ion transfer capability of polymer electrolyte toward Ni-rich-based lithium metal batteries. *Small. Methods.* **6**, 2200258 (2022).
31. F. Rizzo, N. S. Kehr, Recent advances in injectable hydrogels for controlled and local drug delivery. *Adv. Healthc. Mater.* **10**, 2001341 (2021).
32. B. Lotz, Crystal polymorphism and morphology of polylactides, in. *Synthesis, Structure and Properties of Poly(lactic acid)*, M. Di Lorenzo, R. Androsch, Eds. (Springer, 2017), pp. 273–302.
33. Q. Xie, L. Han, G. Shan, Y. Bao, P. Pan, Polymorphic crystalline structure and crystal morphology of enantiomeric poly(lactic acid) blends tailored by a self-assemblable aryl amide nucleator. *ACS. Sustain. Chem. Eng.* **4**, 2680–2688 (2016).
34. Z. Xiong, F. Liu, A. Gao, H. Lin, X. Yu, Y. Wang, Y. Wang, Investigation of the heat resistance, wettability and hemocompatibility of a polylactide membrane via surface crosslinking induced crystallization. *RSC. Adv.* **6**, 20492–20499 (2016).
35. A. M. El-Hadi, Increase the elongation at break of poly (lactic acid) composites for use in food packaging films. *Sci. Rep.* **7**, 46767 (2017).
36. H. Alenezi, M. E. Cam, M. Edirisinghe, Core–sheath polymer nanofiber formation by the simultaneous application of rotation and pressure in a novel purpose-designed vessel. *Appl. Phys. Rev.* **8**, 041412 (2021).
37. M. Liu, S. Wang, L. Jiang, Nature-inspired superwettability systems. *Nat. Rev. Mater.* **2**, 17036 (2017).
38. H. S. Jung, M. H. Kim, J. Y. Shin, S. R. Park, J. R. Jung, W. H. Park, Electrospinning and wound healing activity of β-chitin extracted from cuttlefish bone. *Carbohyd. Polym.* **193**, 205–211 (2018).
39. R. Li, Y. Shi, M. Alsaedi, M. Wu, L. Shi, P. Wang, Hybrid hydrogel with high water vapor harvesting capacity for deployable solar-driven atmospheric water generator. *Environ. Sci. Technol.* **52**, 11367–11377 (2018).
40. J. Qiu, J. Guo, H. Geng, W. Qian, X. Liu, Three-dimensional porous graphene nanosheets synthesized on the titanium surface for osteogenic differentiation of rat bone mesenchymal stem cells. *Carbon.* **125**, 227–235 (2017).

41. J. S. Kang, S. Kim, D. Y. Chung, Y. J. Son, K. Jo, X. Su, M. J. Lee, H. Joo, T. A. Hatton, J. Yoon, Y. E. Sung, Rapid inversion of surface charges in heteroatom-doped porous carbon: A route to robust electrochemical desalination. *Adv. Funct. Mater.* **30**, 1909387 (2020).
42. D. Lu, T. Zhang, L. Gutierrez, J. Ma, J. P. Croué, Influence of surface properties of filtration-layer metal oxide on ceramic membrane fouling during ultrafiltration of oil/water emulsion. *Environ. Sci. Technol.* **50**, 4668–4674 (2016).
43. S. Yu, H. Pang, S. Huang, H. Tang, S. Wang, M. Qiu, Z. Chen, H. Yang, G. Song, D. Fu, B. Hu, X. Wang, Recent advances in metal-organic framework membranes for water treatment: A review. *Sci. Total. Environ.* **800**, 149662 (2021).
44. K. Li, J. Ju, Z. Xue, J. Ma, L. Feng, S. Gao, L. Jiang, Structured cone arrays for continuous and effective collection of micron-sized oil droplets from water. *Nat. Commun.* **4**, 2276 (2013).
45. G. Zhang, B. Li, Y. Zhou, X. Chen, B. Li, Z. Y. Lu, L. Wu, Processing supramolecular framework for free interconvertible liquid separation. *Nat. Commun.* **11**, 425 (2020).
46. X. Q. Cheng, Y. Jiao, Z. Sun, X. Yang, Z. Cheng, Q. Bai, Y. Zhang, K. Wang, L. Shao, Constructing scalable superhydrophobic membranes for ultrafast water–oil separation. *ACS. Nano.* **15**, 3500–3508 (2021).
47. S. Zhang, G. Jiang, S. Gao, H. Jin, Y. Zhu, F. Zhang, J. Jin, Cupric phosphate nanosheets-wrapped inorganic membranes with superhydrophilic and outstanding anticrude oil-fouling property for oil/water separation. *ACS. Nano.* **12**, 795–803 (2018).
48. S. Kim, K. Kim, G. Jun, W. Hwang, Wood-nanotechnology-based membrane for the efficient purification of oil-in-water emulsions. *ACS. Nano.* **14**, 17233–17240 (2020).
49. Z. Chen, D. Zhang, F. Peng, J. Ding, 3D-printed ceramic structures with in situ grown whiskers for effective oil/water separation. *Chem. Eng. J.* **373**, 1223–1232 (2019).
50. Y. Cai, D. Chen, N. Li, Q. Xu, H. Li, J. He, J. Lu, A self-cleaning heterostructured membrane for efficient oil-in-water emulsion separation with stable flux. *Adv. Mater.* **32**, 2001265 (2020).
51. M. Joo, J. Shin, J. Kim, J. B. You, Y. Yoo, M. J. Kwak, M. S. Oh, S. G. Im, One-step synthesis of cross-linked ionic polymer thin films in vapor phase and its application to an oil/water separation membrane. *J. Am. Chem. Soc.* **139**, 2329–2337 (2017).
52. J. Gu, H. Fan, C. Li, J. Caro, H. Meng, Robust superhydrophobic/superoleophilic wrinkled microspherical MOF@rGO composites for efficient oil–water separation. *Angew. Chem. Int. Ed.* **131**, 5351–5355 (2019).
53. Y. Liu, W. Li, C. Yuan, L. Jia, Y. Liu, A. Huang, Y. Cui, Two-dimensional fluorinated covalent organic frameworks with tunable hydrophobicity for ultrafast oil–water separation. *Angew. Chem. Int. Ed.* **134**, e202113348 (2021).
54. S. K. Hong, S. Bae, H. Jeon, M. Kim, S. J. Cho, G. Lim, An underwater superoleophobic nanofibrous cellulosic membrane for oil/water separation with high separation flux and high chemical stability. *Nanoscale* **10**, 3037–3045 (2018).
55. J. Ge, D. Zong, Q. Jin, J. Yu, B. Ding, Biomimetic and superwettable nanofibrous skins for highly efficient separation of oil-in-water emulsions. *Adv. Funct. Mater.* **28**, 1705051 (2018).
56. Y. Liu, X. Wang, S. Feng, Nonflammable and magnetic sponge decorated with polydimethylsiloxane brush for multitasking and highly efficient oil–water separation. *Adv. Funct. Mater.* **29**, 1902488 (2019).
57. Y. Zhao, X. Yang, Z. Cheng, C. H. Lau, J. Ma, L. Shao, Surface manipulation for prevention of migratory viscous crude oil fouling in superhydrophilic membranes. *Nat. Commun.* **14**, 2679 (2023).
58. S. Nizamoglu, M. C. Gather, M. Humar, M. Choi, S. Kim, K. S. Kim, S. K. Hahn, G. Scarcelli, M. Randolph, R. W. Redmond, S. H. Yun, Bioabsorbable polymer optical waveguides for deep-tissue photomedicine. *Nat. Commun.* **7**, 10374 (2016).
59. T. P. Haider, C. Völker, J. Kramm, K. Landfester, F. R. Wurm, Plastics of the future? The impact of biodegradable polymers on the environment and on society. *Angew. Chem. Int. Ed.* **58**, 50–62 (2019).
60. M. Li, X. Gao, X. Wang, S. Chen, J. Yu, Wettable and flexible silica nanofiber/bead-based membranes for separation of oily wastewater. *ACS. Appl. Nano. Mater.* **4**, 2952–2962 (2021).
61. S. H. Yousefi, H. V. Tafresh, Modeling electrospun fibrous structures with embedded spacer particles: Application to aerosol filtration. *Sep. Purif. Technol.* **235**, 116184 (2020).
62. L.-T. Lim, A. C. Mendes, L. S. Chronakis, Electrospinning and electrospraying technologies for food applications. *Adv. Food. Nutr. Res.* **88**, 167–234 (2019).
63. D. N. Phan, M. Q. Khan, N. T. Nguyen, T. T. Phan, A. Ullah, M. Khatri, N. N. Kien, I. S. Kim, A review on the fabrication of several carbohydrate polymers into nanofibrous structures using electrospinning for removal of metal ions and dyes. *Carbohyd. Polym.* **252**, 117175 (2021).
64. P. Jariyasakoolroj, N. Rojanaton, L. Jarupan, Crystallization behavior of plasticized poly(-lactide) film by poly(l-lactic acid)-poly(ethylene glycol)-poly(l-lactic acid) triblock copolymer. *Polym. Bull.* **77**, 2309–2323 (2020).
65. S. Jia, D. Yu, Y. Zhu, X. Su, Z. Wang, L. Chen, A feasible strategy to constructing hybrid conductive networks in PLA-based composites modified by CNT-d-RGO particles and PEG for mechanical and electrical properties. *Polym. Adv. Technol.* **31**, 699–712 (2020).
66. F. Zhang, M. W. King, Biodegradable polymers as the pivotal player in the design of tissue engineering scaffolds. *Adv. Healthc. Mater.* **9**, 1901358 (2020).

Acknowledgments: We would like to thank Editage (www.editage.cn) for English language editing. **Funding:** This work was supported by the National Natural Science Foundation of China (21905067 and 22178076), the Natural Science Foundation of Heilongjiang Province for Distinguished Young Scholars (JQ2020B001), the Heilongjiang Touyan Team (HITTY-20190033), and the State Key Laboratory of Urban Water Resource and Environment (Harbin Institute of Technology) (no. 2022TS43). **Author contributions:** L.S. and X.C. designed the membrane, performed the experiments, analyzed the results, and wrote the manuscript. All authors participated in the analysis of the experimental results and writing of the manuscript. **Competing interests:** All the authors declare that they have no competing interests. **Data and materials availability:** All data needed to evaluate the conclusions in the paper are present in the paper and/or the Supplementary Materials.

Submitted 15 March 2023
Accepted 21 July 2023
Published 23 August 2023
10.1126/sciadv.adh8195